EINDHOVEN UNIVERSITY OF TECHNOLOGY

Measurement and analysis of temperature-dependent optical modal gain in single-layer InAs/InP(100) quantum-dot amplifiers in the 1.6- to 1.8-μm wavelength range

Citation for published version (APA):
Jiao, Y., Veldhoven, van, P. J., Smalbrugge, E., Smit, M. K., He, S., & Bente, E. A. J. M. (2012). Measurement and analysis of temperature-dependent optical modal gain in single-layer InAs/InP(100) quantum-dot amplifiers in the 1.6- to 1.8-μm wavelength range. *IEEE Photonics Journal*, *4*(6), 2292-2306. https://doi.org/10.1109/JPHOT.2012.2231063

DOI:
10.1109/JPHOT.2012.2231063

Document status and date:
Published: 01/01/2012

Document Version:
Accepted manuscript including changes made at the peer-review stage

Please check the document version of this publication:

• A submitted manuscript is the version of the article upon submission and before peer-review. There can be important differences between the submitted version and the official published version of record. People interested in the research are advised to contact the author for the final version of the publication, or visit the DOI to the publisher's website.
• The final author version and the galley proof are versions of the publication after peer review.
• The final published version features the final layout of the paper including the volume, issue and page numbers.

Link to publication

General rights
Copyright and moral rights for the publications made accessible in the public portal are retained by the authors and/or other copyright owners and it is a condition of accessing publications that users recognise and abide by the legal requirements associated with these rights.

• Users may download and print one copy of any publication from the public portal for the purpose of private study or research.
• You may not further distribute the material or use it for any profit-making activity or commercial gain
• You may freely distribute the URL identifying the publication in the public portal.

If the publication is distributed under the terms of Article 25fa of the Dutch Copyright Act, indicated by the “Taverne” license above, please follow below link for the End User Agreement:

www.tue.nl/taverne

Take down policy
If you believe that this document breaches copyright please contact us at:

openaccess@tue.nl

providing details and we will investigate your claim.

Download date: 05. Oct. 2023

Measurement and analysis of temperature-dependent optical modal gain in single-layer InAs/InP(100) quantum dot amplifiers in the 1.6 to 1.8 μm wavelength range

Y. Jiao, [1, 2] ***Student Member, IEEE*****, P.J. van Veldhoven,** [1] **E. Smalbrugge,** [1] **M.K. Smit,** [1] ***Fellow, IEEE*****,**
S. He, [2] ***Senior Member, IEEE*****, and E.A.J.M. Bente,** [1] ***Member, IEEE***

[1]COBRA Research Institute, Eindhoven University of Technology, Eindhoven, 5600 MB, the Netherlands
[2]Centre for Optical and Electromagnetic Research, Zhejiang University, Hangzhou, 310058, China

Corresponding author: Yuqing Jiao (y.jiao@tue.nl)

Abstract: In this paper measurements and analysis of the small signal net modal gain of single-layer InAs/InP(100) quantum dot optical amplifiers are presented. The amplifiers use only a single layer of InAs quantum dots on top of a thin InAs quantum well. The devices have been fabricated using a layer stack that is compatible with active-passive integration scheme which makes further integration possible. The measurement results show sufficient optical gain in the amplifiers and can thus be used in applications such as lasers for long-wavelength optical coherence tomography and gas detection. The temperature dependence of the modal gain is also characterized. An existing rate equation model was adapted and has been applied to analyze the measured gain spectra. The current injection efficiency has been introduced in the model to obtain a good fit with the measurement. It is found that only a small portion (~ 1.7 %) of the injected carriers is actually captured by the QDs. The temperature dependence of several parameters describing the QDs is also discovered. The mechanisms causing the blue shift of peak gain as the current density increases and the temperature changes are analyzed and discussed in detail.

Index Terms: quantum dot (QD), semiconductor optical amplifier (SOA), optical gain, rate equation (RE) model.

1. Introduction

Semiconductor quantum dot (QD) material has attracted great interest among researchers. Because of the three-dimensional confinement of carriers, QD semiconductor optical amplifiers (QD-SOAs) and QD lasers have several advantages over bulk or quantum well (QW) devices. Low threshold current density [1], [2] in QD lasers and ultrafast carrier capture dynamics [3], [4] in QD-SOAs have been experimentally demonstrated. The QD-based devices can also benefit from the inhomogeneous broadening of the QDs. Due to the inhomogeneous size distribution of the QDs, the emission bandwidth can be as wide as 100 – 200 nm [5], which is suitable for applications requiring a wide operating range such as widely tunable lasers. More importantly, the QD material has an advantage in that there is a direct control mechanism for the central emission wavelength over a wide range. The emission wavelength of a single QD is mainly determined by the gap of energy levels and to a limited extent by the width of homogeneous broadening [6]. The wavelength of the photon emitted by the QD can be mainly controlled by the size of the QD which directly determines the energy gap [7]. The average size of the QDs can be controlled during the growth process, which has been demonstrated in the InAs/InP(100) QD platform [8]. Thus the central wavelength of the emission spectra can be tuned from 1.4 μm up to 2 μm.

The wavelength range from 1.6 to 1.8 μm is desirable for several applications such as monolithically integrated tunable lasers [9] and photodetectors [10] used in optical coherence tomography (OCT) or gas detection [11]. The InAs/InP(100) QD platform with QDs tuned to 1.7 μm with wide bandwidth, in combination with the butt-joint active-passive photonic integration scheme [12] can be used for the development of integrated optical devices for 1.6 to 1.8 μm long-wavelength applications.

In our previous work, a five-layer InAs/InP(100) QD material system at 1.6 to 1.8 μm wavelength range has been characterized [13] and successfully used in a tunable laser [9] and a photodetector [10]. The measured small signal net modal gain is relatively low (peak gain of 6.5 cm^{-1} at 3000 A/cm^{-2} at 288 K) compared to bulk or QW materials. This relatively low gain has limited the performance of the tunable laser which operated just above the threshold due to the high intra-cavity loss. One way to improve the output power and tuning speed of the laser is to use a new QD material with higher gain.

In this paper, we present measurement results and their analysis of QD-SOAs based on a single-layer InAs/InP(100) QD platform. This single-layer material is based on a QD-on-QW system (similar to the concepts previously reported in [1], [14]) which shows superior properties as compared to the five-layer QD-SOAs used in our previous experiments. When this single-layer QD amplifier is used in Fabry-Perot ridge waveguide lasers it shows a higher slope efficiency than the one that was achieved with the previously used five-layer QD-SOAs [15]. The small signal gain spectra of the single-layer QD-SOAs have been characterized by us for a series of injection current densities and chip temperatures. The improvement of the optical gain is demonstrated and quantified. An improved rate equation (RE) model based on [13] is applied to model the amplifiers and obtain insight into its operation. From this modeling it is found that only a small fraction of the injected carriers are captured by the QDs. Good fitting to the measured data could be obtained by introducing a high carrier escape rate from

the SCH layer. The resulting low current injection efficiency and high gain contribution from individual QD together determine the absolute value and shape of the gain spectra at different current densities. By fitting the simulation to the measurement, the temperature dependence of the carrier dynamics and several physical parameters in the QDs has been extracted. A number of the parameters in the model turned out to be significantly temperature-dependent. Significant blue shift of the peak gain with increasing carrier density and decreasing temperature was observed and its origin is explained by the model.

The accurate measurement of the gain properties of InAs/InP QDs performed in this work is important for further device optimization, as well as for providing comparison of the gain properties of this active region with those of alternative methods based on other active regions. Prior works had reported the uses of InAs/GaAs QDs [16], [17] for lasers in the 1.2-1.3 µm wavelength region, strained InGaAs QWs [18], [19] and InGaAsSb QWs [20] for achieving long wavelength lasers up to 2.3 µm. Our preference of using QDs as the active material stems from the wider gain bandwidth that QDs can provide compared to the QWs. The wide gain bandwidth is crucial for a widely tunable laser in a swept-source OCT system.

This paper is organized as follows. In Section 2, the device design and fabrication as well as the measurement method are introduced. The measurement results of the small signal gain spectra will be presented in Section 3. The improved RE model will be presented in Section 4, followed by fitting results and analysis in Section 5.

2. Gain characterization method, device design, fabrication

The Hakki-Paoli technique [21] is a well-known method for measuring optical gain. This technique is based on the analysis of resonance modulation in the amplified spontaneous emission (ASE) spectra from a Fabry-Perot cavity operating below threshold. Since the QD-SOAs have a low modal gain compared to bulk or QW materials, the devices have to be several millimeters long in order to provide a sufficient optical gain value that is suitable for measurement. To resolve the closely spaced spectral modes of the modulated ASE spectra of millimeter-long cavities in the 1.6 to 1.8 µm wavelength range a high resolution spectrometer is required which is not available. This makes that the Hakki-Paoli technique is not practical for characterization of these QD-SOAs. The measurement method used in this paper is based on the analysis of ASE spectra from SOAs of different lengths [13], [22]. Only a moderate spectral resolution of the spectrometer is required for this method.

The relation between the ASE output power $P(\lambda,L)$, the net modal gain $G(\lambda)$ of the SOA and the device length L under the condition of no optical feedback and no gain saturation can be written as [23]:

$$P(\lambda,L)=\frac{P_{sp}(\lambda)}{G(\lambda)}\left(e^{G(\lambda)L}-1\right) \tag{1}$$

where $P_{sp}(\lambda)$ is the spontaneous emission power per unit length. The gain can be obtained by fitting a series of ASE spectra from SOAs with different lengths to Eq. (1) at each wavelength.

We have implemented this method by fabricating a series of shallowly etched ridge waveguide amplifiers of various lengths that have been divided into two sections on a single chip. One part is the optical amplifier from which the ASE output is monitored through a cleaved facet. The other section is reverse biased and acts as an absorber which prevents detectable feedback into the amplifier. The advantage of this method is that the random noise and measurement errors such as variation in fiber coupling efficiency can be averaged out when using a sufficiently large number of SOA sections.

In this paper, a chip with a width of 7 mm is used, where the length of SOA sections vary from 4.97 mm to 6.65 mm, as shown in Fig. 1(a). The devices cover a 7 mm × 7 mm area of a 13 mm × 12 mm mask that was used on a quarter of a two inch wafer. The absorber waveguide sections have only 300 nm thick evaporated metal contacts. The isolation sections are etched into the waveguide ridge to provide electrical isolation between the SOA and absorber sections.

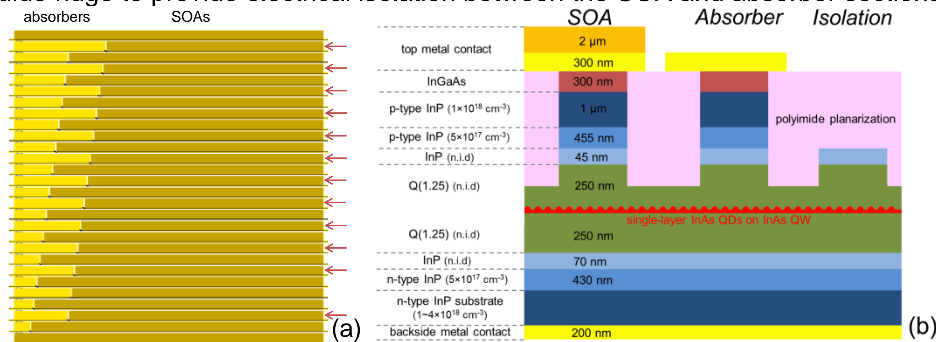

Fig. 1. (a) The layout of a chip with 26 devices with different lengths. The selected devices for the measurement are marked by red arrows. (b) The cross-section structure of the single-layer InAs/InP(100) QD-SOA section, absorber section and isolation section.

The cross-section structure of the single-layer InAs/InP(100) QD-SOAs as well as absorber and isolation sections are presented in Fig. 1(b). The devices are fabricated using a process technology which is fully compatible with the active-passive photonic integration scheme of the COBRA Research Institute [13]. The layer structures are grown by low-pressure metal-organic vapor-phase epitaxy (MOVPE) starting from an n-type InP(100) two inch diameter substrate. The InAs QDs are grown on a thin (1.6 nm) InAs QW layer [15], and are inserted in the center of a 500 nm thick InGaAsP (Q1.25) waveguiding layer as shown in Fig. 1(b). The thickness of the InAs QW layer is designed to control the average size of the InAs QDs to have an emission wavelength around 1.7 µm. The waveguiding layer is sandwiched by a 500 nm n-type InP

bottom cladding and a 1.5 μm p-type InP top cladding with compositionally graded 300 nm p-type InGaAs contact layer. The single-mode shallowly etched waveguides with a width of 2 μm are formed by etching 100 nm into the waveguiding layer using an inductively coupled plasma reactive ion etching (ICP-RIE) process. The isolation section is formed by etching away most of the highly doped p-type top cladding between the SOA and the absorber using the same etching process. All the structures are planarized using polyimide. Metal contacts (TiPtAu) are evaporated at both sides to form electrical contacts. A thick (1.7 μm) Au layer is also plated on top of the evaporated metal contacts of SOAs to reduce the contact resistance and guarantee good spreading of the injected current. The chip is cleaved perpendicular to the waveguides and no coating is applied on the facets. The chip is finally mounted on a copper chuck and contacted with probes. The temperature just beneath the chip is controlled by liquid cooling using a chiller. In order to prevent condensation of water on the chip when temperature is below 283 K, the setup is sealed in an enclosure with a nitrogen atmosphere. The ASE spectra have been obtained by injecting a current into the SOA sections and by collecting the ASE from the facet with a lensed fiber. The absorber sections are reverse-biased at -3 V to prevent optical feedback. The spectra have been recorded using a spectrometer (Yokogawa AQ6375) with 0.5 nm resolution over 400 nm wavelength band around 1.7 μm.

Data from twelve out of the 26 devices are selected to be used in the fitting calculation (marked by red arrows in Fig. 1(a)). The remaining SOAs could not be used due to a non-uniformity in the thickness of the electro-plated gold layer except for one where a defect in the waveguide was observed. In the chip layout (Fig. 1(a)) it can be seen that the relatively long SOA sections are alternated with relatively short SOA sections. Thus a short part of the longer SOAs lies in between un-plated absorber sections. It was clearly visible on the fabricated chip that the deposition of gold in these short parts of the SOAs was much thinner than in the other regions. Thus the current distribution in those relatively long SOAs is not optimal. It was observed that the ASE power for those relatively long SOAs with non-optimal plated gold was consistently too low compared to the selected devices. On the other hand the plating thickness of the selected SOAs was uniform.

3. Gain characterization results

The net modal gain spectra of the single-layer QD-SOAs have been derived from the measurement results of continuous wave (CW) ASE spectra at a range of injection current densities (from 500 A/cm^2 to 5000 A/cm^2 with 500 A/cm^2 increments) and at four different chip temperatures (from 273 K to 303 K with 10 K increment). As an example of the recorded data the ASE spectra obtained from a 5.6 mm-long SOA section are given in Fig. 2(a) for a selection of different injection current densities and chip temperatures. It is obvious from the figure that the ASE power increases as the current density increases. A significant increase of ASE power is also observed as the temperature decreases. It indicates a strong temperature-dependent modal gain of the QD-SOAs. No clear spectral features from contributions of different states in the QD can be seen even at high current densities. This is analogous as reported in [13] for a five-layer InAs/InP QD system. There are spectral features at wavelengths beyond 1800 nm due to absorption of water vapor in the spectrometer. This is not clearly visible in Fig. 2(a) due to the scale of the axis but the effect can be clearly observed in the gain spectra. From the figure it can be clearly seen that both an increase in injection current density and a decrease of chip temperature can result in a blue shift of peak wavelength of the ASE spectra. The observed peak wavelengths as a function of injection current density (from 500 to 5000 A/cm^2 with 500 A/cm^2 increments) and chip temperature (273, 283, 293 and 303 K) are presented in Fig. 2(b). The blue shift of the peak wavelength can be as large as 120 nm for a current density variation of 500 A/cm^2 to 5000 A/cm^2. The blue shift related to the temperature decrease from 303 K to 273 K is approximately 30 nm.

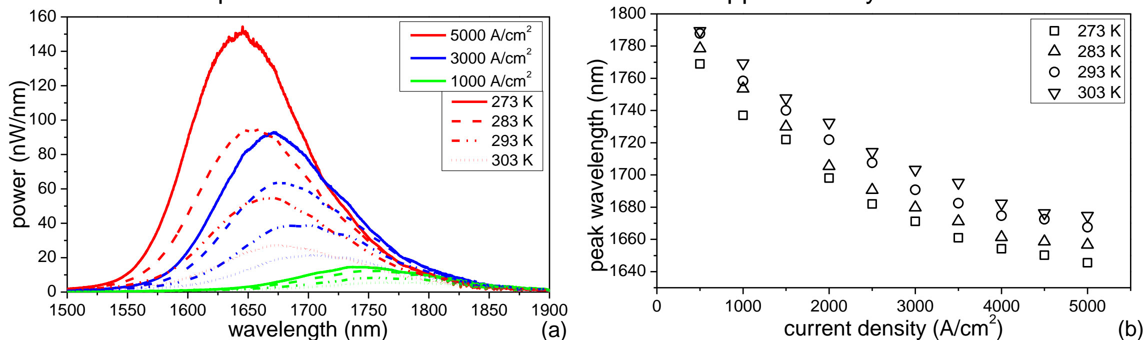

Fig. 2. (a) The measured ASE spectra of the 5.6 mm-long SOA section for a selection of different injection current densities (1000, 3000 and 5000 A/cm^2) and four different chip temperatures (273, 283, 293 and 303 K). (b) The peak wavelengths of ASE spectra of the 5.6 mm-long SOA section under different injection current densities (from 500 to 5000 A/cm^2 with a 500 A/cm^2 increment) and four different chip temperatures (273, 283, 293 and 303 K).

In order to verify the assumption of negligible feedback effects in the recorded ASE spectra, the round trip gain in the whole device (SOA and absorber) is evaluated by measuring the low level optical output from the absorber side and comparing it with the output from the SOA side. The most unfavorable condition for the assumption of negligible feedback is the device with the longest SOA section (5.81 mm) and the shortest absorber section (1.19 mm) at the highest current density (5000 A/cm^2) that has been used. From the observed power level behind the absorber section the total round trip gain is calculated to be -18 dB at 293 K and -14 dB at 283 K. This indicates that the contribution of back-reflected light to the total ASE power is less than 2 % at 293 K and less than 4% at 283 K. The optical feedback is thus sufficiently low to be negligible. The round trip gain at 273 K could not be measured because the size of the sealed enclosure of the set-up is

designed for fiber aligning only at one side.

A nonlinear least square algorithm is used to fit the parameters in Eq. (1) to the measured ASE spectra [13]. A few examples of fitted results and the measured ASE data with the estimated 10 % error bars are presented in Fig. 3. This error value is the upper limit of the variation of the collected ASE power (e.g., due to fiber misalignment) as observed from repeated measurements. The algorithm has taken the 10 % error into account by assigning a weighting factor to each data point. Besides the 12 data points, a zero-length point is also used. The optical power at zero length is chosen as the background noise of the spectrometer. The modal gain spectra can be constructed by calculating the gain value for each wavelength at a certain injection current density and temperature.

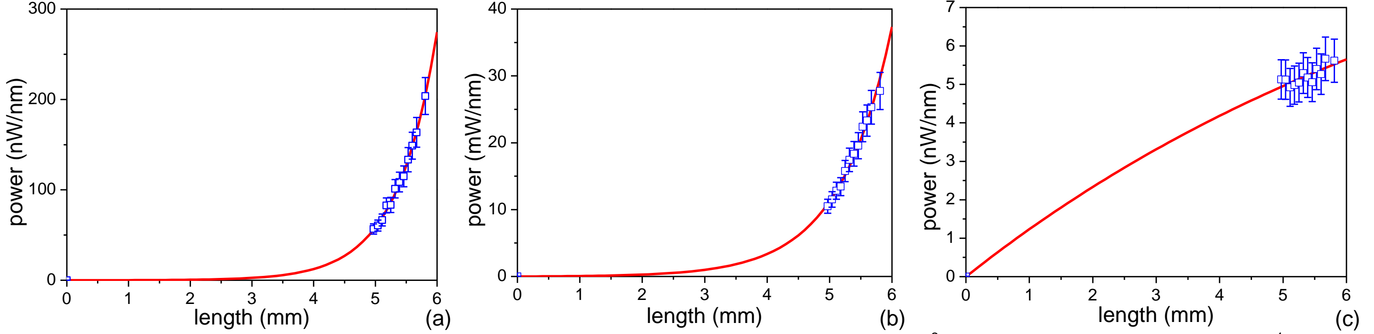

Fig. 3. The fitted ASE power, measured data and the 10 % error bars for (a) λ = 1650 nm, I = 5000 A/cm^2, T = 273 K and fitted G = 15.46 cm^{-1}. (b) λ = 1650 nm, I = 5000 A/cm^2, T = 303 K and fitted G = 11.99 cm^{-1}. (c) λ = 1750 nm, I = 1000 A/cm^2, T = 303 K and fitted G = -1.16 cm^{-1}.

The net modal gain of the single-layer InAs/InP(100) QD-SOAs is first derived for different injection current densities at a fixed chip temperature, as shown in Fig. 4. The net modal gain spectra at 273 K are plotted for full range of injection current densities (from 500 to 5000 A/cm^2 with a 500 A/cm^2 increment) in Fig. 4(a). The net modal gain spectra with 68 % confidence bounds at 273 K are plotted for five selected injection current densities in Fig. 4(b). From the figures a blue shift of peak wavelengths of the gain spectra similar to the ASE spectra can be observed as the injection current density increases. The distortion of the gain spectra above 1750 nm is mainly due to the absorption by the water vapor in the air inside the spectrometer. The recorded optical power at wavelengths close to the water absorption peaks is not accurate due to the relatively low resolution (0.5 nm) used in the measurement.

The net modal gain spectra are also plotted for different chip temperatures. As can be seen in Fig. 5, the peak value of the gain increases significantly as the temperature drops. The temperature dependence of the peak gain is about 2 cm^{-1} per 10 K at a current density of 5000 A/cm^2. There is also a blue shift of the peak wavelength of the gain as the temperature drops. The lasing wavelength in the QD laser will be strongly dependent on the current injection density and slightly on the operation temperature. The mechanisms that are causing the current-density-dependent and temperature-dependent blue shift will be discussed in Section 5 using a RE model of the amplifiers.

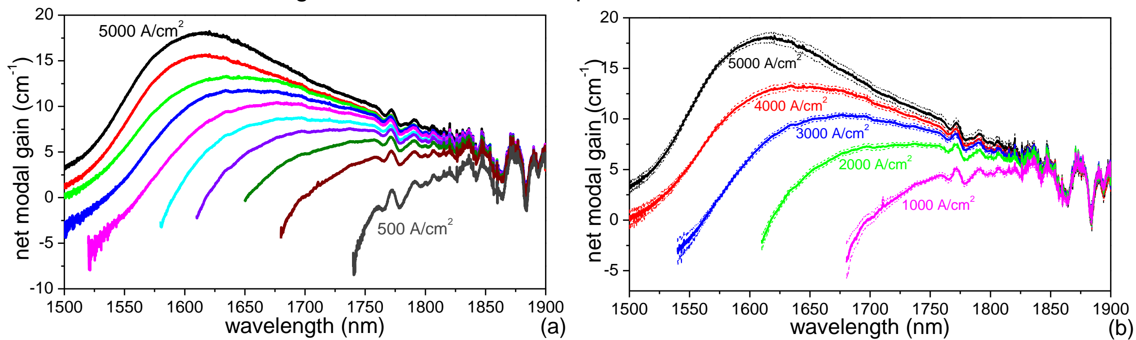

Fig. 4. (a) The measured net modal gain for the full range of injection current densities used (from 500 to 5000 A/cm^2 with a 500 A/cm^2 increment) at 273 K. (b) The measured net modal gain with 68 % confidence bounds at five injection current densities (1000, 2000, 3000, 4000 and 5000 A/cm^2) at 273 K.

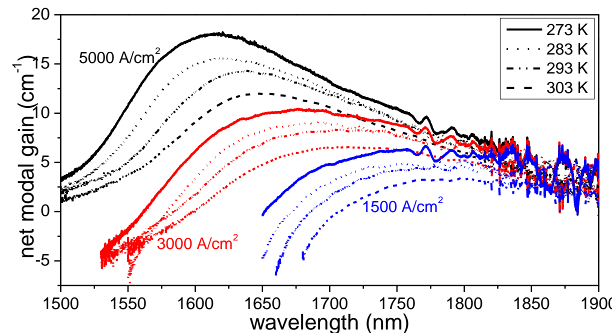

Fig. 5. The net modal gain spectra for different chip temperatures (from 273 K to 303 K with 10 K increment) and three injection current densities (1500, 3000 and 5000 A/cm^2).

4. Improved rate equation model

Several multi-level RE models have been proposed to understand the carrier dynamics and the mechanisms causing the blue shift of the gain spectra in the QD-SOAs [6, 13, 24, 25]. The RE model in [13] has been successfully fitted to the gain spectra of the five-layer InAs/InP(100) QD-SOAs. This model was used to explain how two different mechanisms cause the blue shift of the peak wavelength in the gain spectra of five-layer QD-SOAs as a function of current density. However a good fit to the measured data could not be obtained using this model for the new single-layer InAs/InP(100) QD-SOAs presented here. An example of a result from a net modal gain calculation at 293 K is shown in Fig. 6. The shape of the measured gain spectra can be reproduced using this model. But the dependence of the gain on the current density as measured cannot be described properly. For instance, the difference in peak gain for the fitted gain spectra is 0.7 cm^{-1} between 4000 and 5000 A/cm^2 while the measured difference is 4 cm^{-1}. The main reason of this difference is that the carrier population of the QD as a function of current density is overestimated. In reality the QDs start to be filled up and the population density becomes saturated at much higher injected carrier density values.

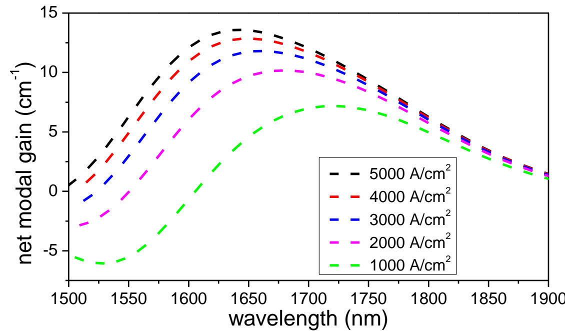

Fig. 6. The fitted gain curve using the RE model presented in [13] at 293 K.

In order to solve this mismatch between the RE model and the measured data, we have modified the RE model presented in [6, 13, 26]. The first of the improvements on the previous RE model is the introduction of the current injection efficiency. This concept of current injection efficiency has been previously applied to study the temperature-dependent carrier leakage out of QW in the InGaAsN QW lasers [27] and the efficiency-droop in the InGaN QW light emitting diodes (LEDs) [28]. Since the active layer of the single-layer QD-SOA is very thin (1 monolayer (ML) of InAs QDs + 1.6 nm InAs QW [15]) compared to the active region in five-layer QD-SOA (200 nm in total [13]), and the layer stack of the active region is different, only a small portion of the injected carriers are collected by the active layer. Unlike the assumed 100 % carrier collection in [13], the improved model includes an additional carrier escape mechanism out of the QD amplifier [29, 30]. This carrier escape rate out of separate confinement heterostructure (SCH) layer of the QD amplifier is assumed to be temperature-dependent due to the thermal mechanism of the escape rate. This escape rate has numerically the same effect as a large carrier recombination rate in the SCH. However, physically the escape rate is much faster than the carrier recombination rate.

Besides several parameters of which the temperature dependence is already defined in the RE model, we also discovered that a temperature dependence of parameters which were previously defined as constants is required. Thus the second improvement is the incorporation in the model for the temperature-dependence of the homogeneous broadening of the QD and the escape rate out of SCH as mentioned above. This is explained in detail in the next section. In this work these parameters are adjusted for different temperatures in the simulation to fit the experimental data.

In the model only the dynamics of electrons is considered since it is assumed that the dynamics of the holes immediately follows that of the electrons. The carrier time constants are thus the same for electrons and holes. The electron energy levels are equal to the transition energies, the energy levels of holes are equal and set to zero. Both homogeneous and inhomogeneous broadening of the QDs as well as the occupation-dependent carrier capture time and the temperature-and-transition-energy-dependent carrier escape time constants are taken into account. Neither the Auger effect in the dots [31] nor direct carrier relaxation from the wetting layer (WL) to the ground state (GS) [31] is included in the model. Since the QD-SOAs are operating below threshold, we assume that the portion of carriers in the GS and excited state (ES) that contribute to spontaneous emission does not influence the total number of carriers much. Thus the equations for photons are not included in the model.

The energy bands and carrier dynamics in a QD for the improved RE model are depicted in Fig. 7. The model contains a SCH where the carriers are injected into and escape out of the QD. The WL acts as a common carrier reservoir. In order to express the effect of the inhomogeneous dot size distribution, the ES and GS of the QD are allocated into N sub-groups with each sub-group representing a certain average dot size (energy level). The carriers are injected into SCH with a constant rate I/e. They can relax to WL with a rate of $1/\tau_s$. Only part of the carriers is captured by the QD, the rest flow through the SCH layer with a rate of $1/\tau_{esc}$ (this corresponds to the first improvement to the RE model). The carriers in the WL can be captured by the ES with a rate of $1/\tau_c$ or escape back to the SCH with a rate of $1/\tau_{qe}$. Carriers in the ES can relax to GS with a rate of $1/\tau_d$ or escape back to WL with a rate of $1/\tau_{eES}$. In the GS, the carriers can escape back to ES with a rate of $1/\tau_{eGS}$. In all energy states, the carriers will experience carrier loss processes (radiative and non-radiative) with rates of $1/\tau_{sr}$ for SCH, $1/\tau_{qr}$ for WL and $1/\tau_r$ for ES and GS.

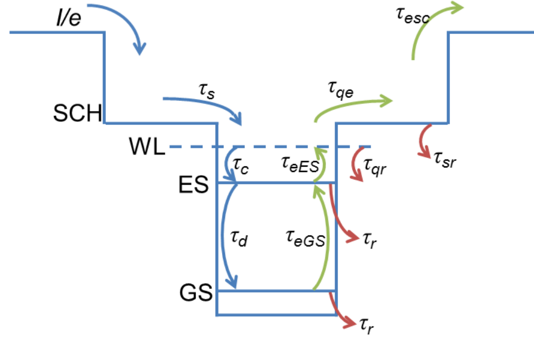

Fig. 7. The schematic of the energy band diagram of the QD active region. The carrier dynamics are also indicated. The blue arrows indicate the carrier injection/collection, the green arrows the carrier escape and the red arrows the carrier losses.

The resulting rate equations are as follows:

$$\frac{dN_s}{dt} = \frac{I}{e} + \frac{N_q}{\tau_{qe}} - \frac{N_s}{\tau_s} - \frac{N_s}{\tau_{sr}} - \frac{N_s}{\tau_{esc}(T)}, \tag{2}$$

$$\frac{dN_q}{dt} = \frac{N_s}{\tau_s} + \sum_n \frac{N_{ESn}}{\tau_{eESn}} - \frac{N_q}{\tau_{qr}} - \frac{N_q}{\tau_{qe}} - \frac{N_q}{\tau_{c0}} \sum_n (1 - P_{ESn}) G_n, \tag{3}$$

$$\frac{dN_{ESn}}{dt} = \frac{N_q G_n (1 - P_{ESn})}{\tau_{c0}} + \frac{N_{GSn}(1 - P_{ESn})}{\tau_{eGSn}} - \frac{N_{ESn}}{\tau_r} - \frac{N_{ESn}}{\tau_{eESn}} - \frac{N_{ESn}(1 - P_{GSn})}{\tau_{d0}}, n = 0, 1, \ldots, N-1, \tag{4}$$

$$\frac{dN_{GSn}}{dt} = \frac{N_{ESn}(1 - P_{GSn})}{\tau_{d0}} - \frac{N_{GSn}}{\tau_r} - \frac{N_{GSn}(1 - P_{ESn})}{\tau_{eGSn}}, n = 0, 1, \ldots, N-1. \tag{5}$$

where N_s is the number of carriers in SCH, N_q the number of carriers in WL, N_{ESn} the number of carriers in the n-th sub-group of ES and N_{GSn} the number of carriers in the n-th sub-group of GS. It can be clearly seen that the rate equations consist of one equation for SCH (Eq. (2)), one for WL (Eq. (3)), N for ES (Eq. (4)) and N for GS (Eq. (5)). The carrier escape times of ES τ_{eES} and GS τ_{eGS} are related with the carrier capture times τ_{c0} and τ_{d0} which are the average capture time for empty energy states. The τ_{eES} and τ_{eGS} are also dependent on the transition energy and temperature in the following way:

$$\tau_{eESn} = \tau_{c0} \frac{\mu_{ES} N_D V_A}{\rho_{WLeff} V_{WL}} e^{\frac{E_{WL} - E_{ESn}}{\kappa_B T}}, n = 0, 1, \ldots, N-1, \tag{6}$$

$$\tau_{eGSn} = \tau_{d0} \frac{\mu_{GS}}{\mu_{ES}} e^{\frac{E_{ESn} - E_{GSn}}{\kappa_B T}}, n = 0, 1, \ldots, N-1. \tag{7}$$

where $\mu_{ES} = 4$ and $\mu_{GS} = 2$ are the degeneracy of the ES and GS; EWL, E_{ESn} and E_{GSn} the energy levels of the WL and the n-th sub-group of ES and GS; N_D the dot density; ρ_{WLeff} the effective density of states in the WL, V_A and V_{WL} the volume of the QD active region and the WL.

The coupled rate equations (Eq. (2) – Eq. (5)) have been solved in the time domain. They are integrated in time until a steady state has been reached [13]. From the solved parameters, the contribution of the gain from n-th sub-group of QD to the m-th wavelength can be determined by:

$$g_{mnES} = \mu_{ES} C_g \frac{N_w N_D}{H_{act}} \frac{|P_{ES}^{\sigma}|^2}{E_{ESn}} (2P_{ESn} - 1) G_n \cdot B_{cv}(T) \cdot (E_m - E_{ESn}), \tag{8}$$

$$g_{mnGS} = \mu_{GS} C_g \frac{N_w N_D}{H_{act}} \frac{|P_{GS}^{\sigma}|^2}{E_{GSn}} (2P_{GSn} - 1) G_n \cdot B_{cv}(T) \cdot (E_m - E_{GSn}). \tag{9}$$

where C_g is a constant, N_w the number of QD layers, N_D the QD density, H_{act} the total active layer thickness, $|P^{\sigma}_{ES,\,GS}|^2$ the transition matrix elements of ES and GS recombinations [6], G_n the normalized fraction of n-th dot group, $B_{cv}(T)$ the Lorentzian homogeneous broadening function [6] with a temperature-dependent full width half maximum (FWHM) of $2\hbar\Gamma_{cv}(T)$ and E_m the energy of the m-th wavelength. The total net modal gain of the QD-SOA for each m-th wavelength can be calculated as:

$$G_m = \Gamma \sum_n (g_{mnES} + g_{mnGS}) - \alpha_i, m = 0, 1, \ldots, M-1. \tag{10}$$

where Γ is the confinement factor of the QD active layer and α_i the internal modal loss.

The temperature dependences of τ_{eESn} and τ_{eGSn} are already defined in the original model as can be seen in Eq. (6) and (7). As mentioned above the temperature dependences of $\tau_{esc}(T)$ and $2\hbar\Gamma_{cv}(T)$ were not included in the previous model but these are fitted at each temperature for the improved model. These parameters are explicitly indicated in Eq. (2) and Eq. (8) and (9) as a function of temperature.

The current injection efficiency introduced in the improved model can be defined by the ratio of carriers captured by the QD to the escaped carriers, that is,

$$\eta_{injec} = (1 - \frac{N_s / \tau_s}{I / e}) \times 100\% \quad (11)$$

5. Simulation results and analysis

All the values of parameters used in the model are summarized in Table 1. The FWHM of homogeneous and inhomogeneous broadenings are not known for the single-layer QD amplifiers. They are both varied to obtain the best fitting of the simulation to the experiment. The FWHM of the inhomogeneous broadening is determined as a fixed value since the dot size distribution is an intrinsic parameter. The FWHM of homogeneous broadening is dependent on the temperature [32-34], and thus has been fitted separately for each temperature with the results as shown in Fig. 8(a). The homogeneous linewidth of the QD decreases as the temperature decreases. According to our simulation, the slope is about 0.8 meV/K. We set the recombination rate in the SCH (τ_{sr}) to be 4.5 ns which is comparable to other QD systems [13, 26]. The escape rate out of the SCH layer (τ_{esc}) is fitted for each temperature with the results as shown in Fig. 8(b). The fast escape rate represents a low injection efficiency which is calculated to be about 1.7 %. We attribute this low injection efficiency mainly due to the thin active layer. Compared to the simulation results of the unmodified model (Figure 6) the QD-SOAs will then have a lower fraction of the dots populated with carriers at the same current densities. This will result in larger differences of gain values between the gain spectra at different current densities. Since the single-layer QD amplifier has a different layer stack (InAs QDs on thin InAs QW) compared to previous five-layer QD amplifier (five layers of InAs QDs on GaAs interlayer), the gain contribution from an individual QD might be different for the two QD systems. Thus the transition matrix elements are also fitted during simulation. The fitted result shows a higher gain contribution (the transition matrix element is 4 times higher) from individual QD for the single-layer QD amplifier compared to the previous five-layer QDs. The higher modal gain achieved for single-layer QD amplifiers is mainly due to this increase of gain contribution from individual QDs, even when the total density of QDs is much less (3.4×10^{10} cm^{-2}) compared to the five-layer QDs (3.1×10^{10} cm^{-2} in each layer).

The best fit is obtained when both a low injection efficiency and a high individual gain are used in the model. The carrier capture rate from SCH to WL (τ_s) and the recombination rate (τ_{qr}) in the WL are also fitted during simulation because the WL is different for the single-layer QD-SOAs compared to the five-layer QD-SOAs. The rest of the parameters are obtained from literature [6, 13, 26] as indicated in Table 1.

Table 1
Parameter values used in the improved RE model

Simulation parameters	**Value**	**Reference**
FWHM of inhomogeneous broadening	$\Gamma_0 = 80$ meV	Fit
FWHM of homogeneous broadening	6 meV $< 2\hbar\Gamma_{cv} <$ 30 meV	Fit, temperature dependent
Effective density of states in WL	$\rho_{WLeff} = 2.26\times10^{-11}$ cm^{-2} @ 283 K, 2.34×10^{-11} cm^{-2} @ 283 K, 2.43×10^{-11} cm^{-2} @ 293 K, 2.51×10^{-11} cm^{-2} @ 303 K	[13]
Degeneracy of GS	$\mu_{GS} = 2$	
Degeneracy of ES	$\mu_{ES} = 4$	
Relaxation time from SCH to WL	$\tau_s = 6.5$ ns	Fit
Capture time from WL to ES	$\tau_{c0} = 1$ ps	[4]
Capture time from ES to GS	$\tau_{d0} = 1$ ps	[4]
Escape time from SCH out of QD	45 ps $< \tau_{esc} <$ 56 ps	Fit, temperature dependent
Escape time from WL to SCH	$\tau_{qe} = 3$ ns	[26]
Recombination time in SCH	$\tau_{sr} = 4.5$ ns	[26]
Recombination time in WL	$\tau_{qr} = 0.1$ ns	Fit
Recombination time in ES and GS	$\tau_r = 1$ ns	[4]
QD density	$N_D = 3.4\times10^{10}$ cm^{-2}	[15]
Number of QD layer	$N_W = 1$	
Active layer thickness	$H_{act} = 4$ nm	
Refractive Index	$n_r = 3.261$	
Optical confinement factor	$\Gamma = 0.0068$	
Transition matrix elements	$\lvert P^{\sigma}_{ES,GS}\rvert^2 = 12\cdot m_0\cdot E_{ES,GS}$ kg·eV	fit, [6]
Internal modal loss	$\alpha_i = 1$ cm^{-1}	calculated [35]
Temperature	$T = 273, 283, 293, 303$ K	
Number of QD sub-groups	$N = 501$	

Number of wavelength group	$M = 501$	

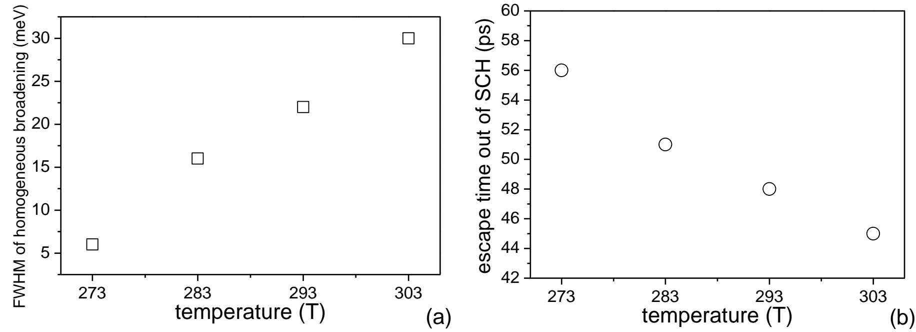

Fig. 8. (a) FWHM of the homogeneous broadening of the QD versus temperature. (b) The carrier escape time out of SCH layer of QD versus temperature.

Two major effects in the single-layer QD amplifiers have been demonstrated to contribute to the blue shift of the peak wavelength of gain spectra due to the increase of current density using a similar analyzing method presented in [13] for five-layer QDs. One effect is the contribution of optical transitions from the ES at higher current density. The carrier captured by a QD will relax to the lowest energy level which contains a free position. If both two positions in the GS are occupied, the carrier will instead fill one of the four positions in the ES. At a low current density, the carriers can relax to GS which corresponds to the gain peak around GS wavelength. When the current density increases to an extent such that all the free positions in GS are fully occupied, the carriers will start to fill in ES. The ES wavelength will start to take over the peak wavelength at a certain current density. The second effect is the dot-size dependent carrier escape rate from QD levels to WL. The carrier escape rates in the ES and the GS are dependent on the energy gap $E_{WL} - E_{ESn}$ and $E_{Esn} - E_{GSn}$. Since the energy level of smaller dots is higher than the energy level in the larger dots, it will be closer to the energy level of WL. Thus the smaller dots will experience a faster escape rate than larger dots. The carrier capture rate from the WL to the QD levels is however not dot-size dependent. As a result, the larger dots with longer wavelengths will be more populated at first due to a slower escape rate. When the current density increases, the smaller dots start to be more populated. The gain spectra will then shift to shorter wavelengths.

Good fitting could be obtained only when both effects are taken in to account in the RE model. The energy levels of the WL, ES and GS are chosen to enable both effects. They are determined to be 1350 nm for WL (E_{WL} = 0.919 eV), 1580 nm for ES (E_{ES} = 0.785 eV) and 1730 nm for GS (E_{GS} = 0.717 eV). The simulations are performed for separate contributions from the ES and GS as well as the total modal gain at four different temperatures (273, 283, 293 and 303 K), as shown in Fig. 9(a) – (h). The measured gain spectra are plotted together with the total simulated gain for easy comparison. As can be seen from Fig. 9(a, c, e, g), both effects that contribute to the blue shift can be observed. As the current density increases, the GS start to be fully occupied which result in saturation in the GS gain. The carriers start to fill in ES and the contribution of ES begins to dominate. The effect of dot-size dependent capture rate can also be seen. Both contributions from ES and GS show slight blue shift as the current density increases. The total simulated modal gain has a good match with the measured gain spectra (Fig. 9(b, d, f, h)). A small deviation between simulation and measured data can be seen at low current densities (1000 and 2000 A/cm^2) for all temperatures. It is probably due to an underestimation of the temperature dependence of the current injection efficiency. In this paper this parameter is adjusted to obtain the best fit for high current densities. In reality the actual temperature inside the QD-SOA is strongly dependent on the injection current density. The simulated modal gain spectra for 1000 and 2000 A/cm^2 can be corrected by adjusting the τ_{esc} to fit with the measured data. After the adjustment, the correction of τ_{esc} corresponds to the injection efficiency η_{injec} of about 2 % for 2000 A/cm^2 and 2.3 % for 1000 A/cm^2. It can also be seen in Fig. 9(b) that the curve for the current density of 4000 A/cm^2 at 273 K deviates considerably. This is also possibly due to an underestimation of the temperature dependence of injection efficiency in the model, or measurement error.

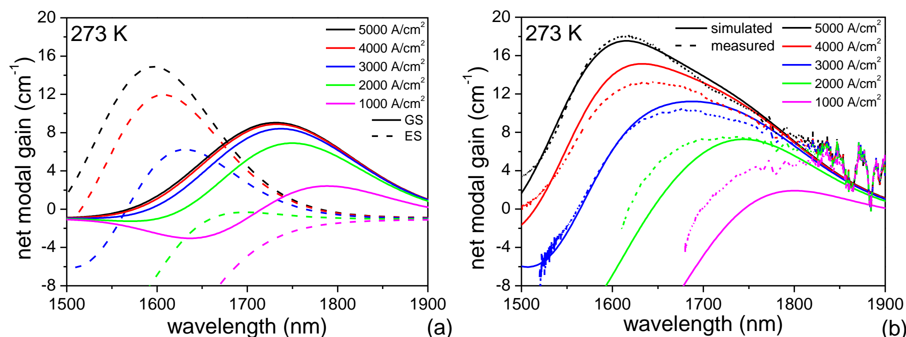

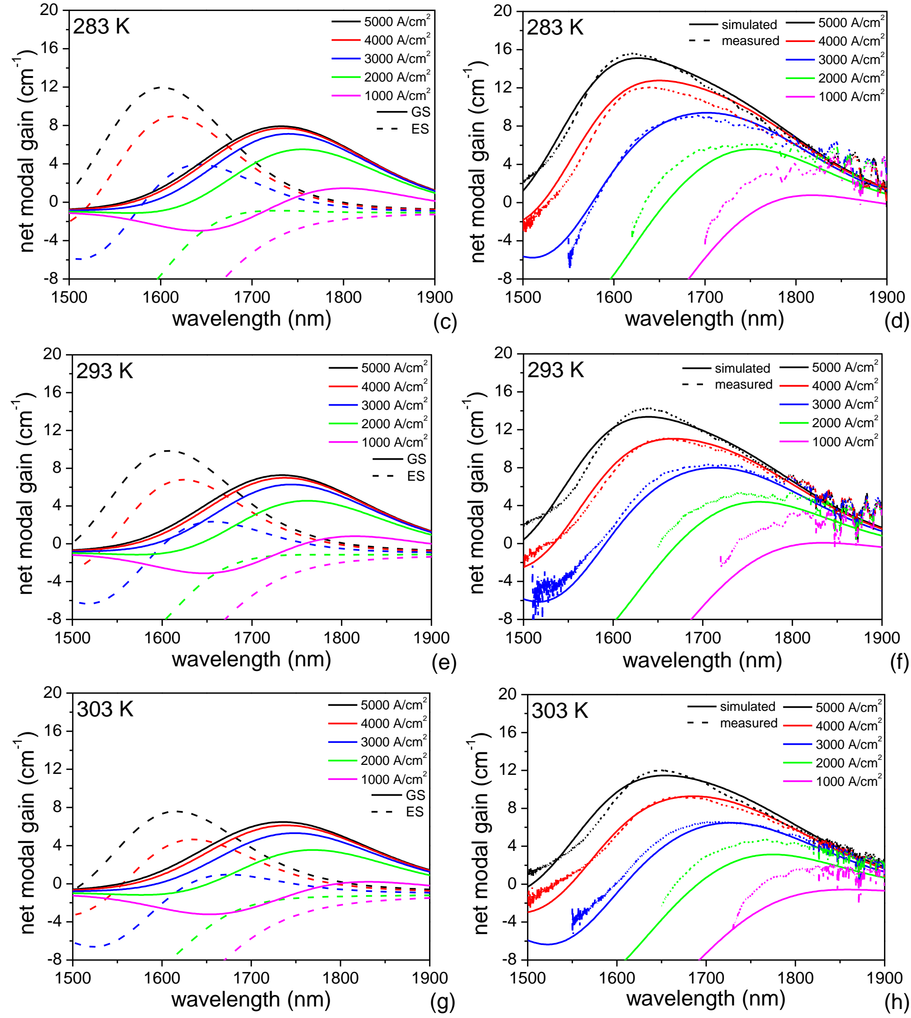

Fig. 9. Simulated modal gain of single-layer QD-SOA. (a, b) 273 K (c, d) 283 K (e, f) 293 K (g, h) 303 K. The contributions from ES and GS for each temperature are shown in the left column (a, c, e, g), the total simulated modal gain and the measured gain spectra are plotted in the right column (b, d, f, h).

The blue shift of the peak wavelength of the gain spectra due to temperature change is also analyzed. The blue shift with respect to the temperature change matches well with the measured data (1 nm/K at 5000 A/cm^2). It is found that there are two mechanisms that contribute to the shift of the peak of the gain spectra.

The first mechanism is due to an increased filling of carriers into smaller QDs as the temperature drops. The occupation probabilities of ES and GS of all the QD sub-groups are plotted for three current densities (1500, 3000 and 5000 A/cm^2) and four temperatures (273, 283, 293 and 303 K) in the graphs in Fig. 10(a) and (b). It should be noticed that the smaller energy of ES or GS of a dot sub-group corresponds to a larger dot size and longer wavelength and the larger energy corresponds to a smaller dot size and shorter wavelength. The change of number of carriers in ES and GS in a certain sub-group is defined by Eq. (4) for ES and Eq. (5) for GS. As can be seen from the equations, the carrier capture rates from WL to ES ($N_q G_n (1-P_{ESn})/\tau_{c0}$) and from ES to GS ($N_{ESn}(1-P_{GSn})/\tau_{d0}$) are dependent on the occupation probabilities of ES and GS of the certain sub-group. When carriers are injected into the amplifier, the larger dots will be more populated than the smaller dots, since the escape rate for larger dots is lower than that of the smaller dots. Thus the carrier capture rates will be lower for larger dots due to a higher occupation probability. As temperature drops, there will be more carriers captured into WL and those carriers will have a higher chance to be captured in smaller dots rather than larger dots since most of the larger dots are already occupied. As a result there are more carriers filling into smaller QDs as temperature drops while the number of carriers filled in larger QDs keep almost the same as shown in Fig. 10(a) and (b). This will result in more contribution of gain from smaller QDs (shorter wavelengths) and the gain peak will shift towards shorter wavelength. This mechanism exists for all range of current densities and temperatures, and for both ES and GS.

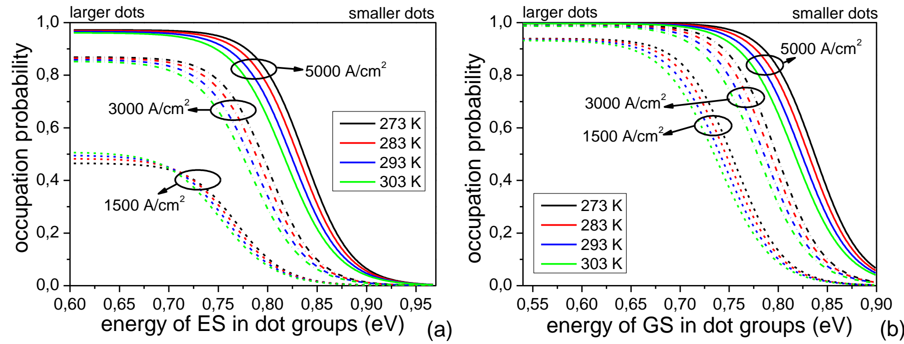

Fig. 10. The occupation probabilities of (a) ES and (b) GS of all the QD sub-groups for three current densities (1500, 3000 and 5000 A/cm^2) and four temperatures (273, 283, 293 and 303 K).

The peak wavelength shift caused by the temperature dependence of the carrier escape rates from QD levels to the WL (see Eq. (6) and (7)) is also investigated. As can be seen from Fig. 7, τ_{eES} and τ_{eGS} determine the escape rates from ES and GS to the WL. The escape time τ_{eES} is plotted for all QD sub-groups and four temperatures in Fig. 11(a) and the τ_{eGS} is not sensitive to the dot size and is only plotted as a function of temperature in Fig. 11(b). It can be seen from Fig. 11(a) that the larger dots will have a larger escape time (slower escape rate) from ES to WL than the smaller dots. As temperature drops, the escape rate for larger dots will decrease more than smaller dots. Thus there will be a higher contribution of gain from larger dots due to this lower escape rate. This will shift the peak of gain to a longer wavelength. Similarly, the temperature-dependent escape rate τ_{eGS} from GS to ES will result in more contribution of gain from GS since the rate will also decrease as temperature drops. This also results in a red shift of the peak of gain.

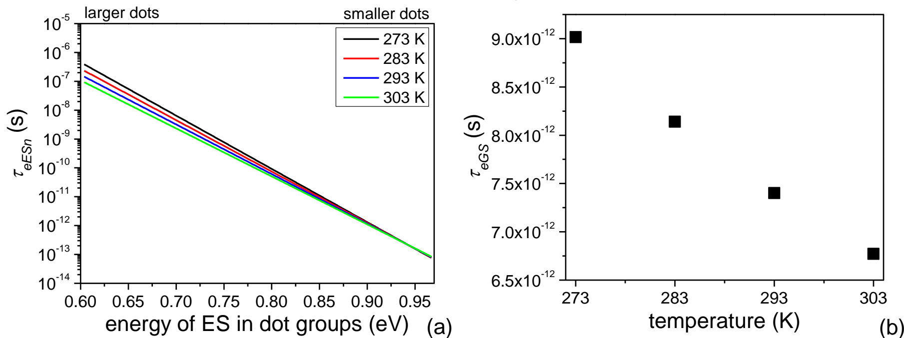

Fig. 11. (a) The escape time τ_{eES} for all QD sub-groups and four temperatures (273, 283, 293 and 303 K). (b) The escape time τ_{eGS} as a function of temperature.

The two mechanisms discussed above both contribute to the shift of the gain peak. But their contributions to the wavelength shift have opposite signs. Since both measurement and simulation show an overall blue shift, it can be concluded that the mechanism of carrier filling is more significant than that of carrier escape when the temperature changes.

6. Conclusion

In this paper we have presented the measured temperature-dependent gain spectra for single-layer InAs/InP(100) QD-SOAs in the 1.6 to 1.8 μm wavelength range. The measurement is realized by analyzing the ASE spectra from QD-SOAs with different lengths at different current densities and chip temperatures. The measured QD-SOAs which are InAs dots grown on a thin InAs layer, show higher gain values than five-layer QD-SOAs with InAs dot on GaAs monolayer. The gain of these InAs QDs-on-QW amplifiers can be further improved by multiple stacking these active layers (similar to what has been done for previous five-layer InAs QDs on GaAs interlayer). However due to the large gain bandwidth that we are after, the gain values are expected to always be lower than those of spectrally more narrow gain QW materials. The blue shift of the peak gain with current density and temperature changes has been analyzed by an improved RE model. A temperature-dependent carrier escape rate from the SCH out of the amplifier is introduced to explain the low current injection efficiency (~ 1.7 %) for the single-layer QD amplifier. The FWHM of the homogeneous broadening of the transitions in the QDs also had to be made temperature dependent in the simulation. The simulations confirmed for the new material that the cause of the blue shift due to increasing current density is a combination of two effects: a transition from GS to ES gain, and dot-size dependent escape rates. The cause of the blue shift with decreasing temperature is also analyzed and found to be determined mainly by two mechanisms: One is the increased carrier filling into smaller dots as temperature drops. The other is the temperature- dependent escape rates from QD levels to WL. The former mechanism results in a blue shift while the latter results in a red shift. The overall blue shift of the gain peak indicates a more significant effect of the former mechanism over the latter one. A good match can be obtained for all temperatures when all effects are taken into account. This type of QD material is a good candidate for utilization in QD lasers or photodetectors for long-wavelength OCT and gas detection applications.

Acknowledgements

The authors thank the support from the BrainBridge project (collaboration between Zhejiang University, Eindhoven University of Technology and Philips Research), China Scholarship Council (CSC) and the NRC Photonics grant.

References

[1] G. Liu, A. Stintz, H. Li, K. J. Malloy, and L. F. Lester, "Extremely low room-temperature threshold current density diode lasers using InAs dots in $In_{0.15}Ga_{0.85}As$ quantum well," *Electronics Letters,* vol. 35, pp. 1163-1165, 1999.

[2] P. Caroff, C. Paranthoen, C. Platz, O. Dehaese, H. Folliot, N. Bertru, C. Labbe, R. Piron, E. Homeyer, A. Le Corre, and S. Loualiche, "High-gain and low-threshold InAs quantum-dot lasers on InP," *Applied Physics Letters,* vol. 87, pp. -, Dec 12 2005.

[3] P. Borri, W. Langbein, J. M. Hvam, F. Heinrichsdorff, M. H. Mao, and D. Bimberg, "Ultrafast gain dynamics in InAs-InGaAs quantum-dot amplifiers," *Photonics Technology Letters, IEEE,* vol. 12, pp. 594-596, 2000.

[4] E. W. Bogaart, R. Nötzel, Q. Gong, J. E. M. Haverkort, and J. H. Wolter, "Ultrafast carrier capture at room temperature in InAs/InP quantum dots emitting in the 1.55 µm wavelength region," *Applied Physics Letters,* vol. 86, p. 173109, 2005.

[5] Z.-z. Sun, D. Ding, Q. Gong, W. Zhou, B. Xu, and Z.-G. Wang, "Quantum-dot superluminescent diode: A proposal for an ultra-wide output spectrum," *Optical and Quantum Electronics,* vol. 31, p. 1235, 1999.

[6] M. Sugawara, K. Mukai, Y. Nakata, H. Ishikawa, and A. Sakamoto, "Effect of homogeneous broadening of optical gain on lasing spectra in self-assembled $In_xGa_{1-x}As$/GaAs quantum dot lasers," *Physical Review B,* vol. 61, pp. 7595-7603, 2000.

[7] M. Holm, M.-E. Pistol, and C. Pryor, "Calculations of the electronic structure of strained InAs quantum dots in InP," *Journal of Applied Physics,* vol. 92, pp. 932-936, 2002.

[8] R. Nötzel, S. Anantathanasarn, R. P. J. van Veldhoven, F. W. M. van Otten, T. J. Eijkemans, A. Trampert, B. Satpati, Y. Barbarin, E. A. J. M. Bente, Y.-S. Oei, T. de Vries, E.-J. Geluk, B. Smalbrugge, M. K. Smit, and J. H. Wolter, "Self assembled InAs/InP quantum dots for telecom applications in the 1.55 µm wavelength range: wavelength tuning, stacking, polarization control, and lasing," *Japanese Journal of Applied Physics,* vol. 45, pp. 6544-6549, 2006.

[9] B. W. Tilma, Y. Jiao, J. Kotani, B. Smalbrugge, H. P. M. M. Ambrosius, P. J. Thijs, X. J. M. Leijtens, R. Nötzel, M. K. Smit, and E. A. J. M. Bente, "Integrated Tunable Quantum-Dot Laser for Optical Coherence Tomography in the 1.7 µm Wavelength Region," *Quantum Electronics, IEEE Journal of,* vol. 48, pp. 87-98, 2012.

[10] Y. Jiao, B. W. Tilma, J. Kotani, R. Nötzel, M. K. Smit, S. He, and E. A. J. M. Bente, "InAs/InP(100) quantum dot waveguide photodetectors for swept-source optical coherence tomography around 1.7 µm," *Opt. Express,* vol. 20, pp. 3675-3692, 2012.

[11] P. Werle, "A review of recent advances in semiconductor laser based gas monitors," *Spectrochimica Acta Part A: Molecular and Biomolecular Spectroscopy,* vol. 54, pp. 197-236, 1998.

[12] H. Wang, J. Yuan, P. J. van Veldhoven, T. de Vries, B. Smalbrugge, E. J. Geluk, E. A. J. Bente, Y. S. Oei, M. K. Smit, S. Anantathanasarn, and R. Notzel, "Butt joint integrated extended cavity InAs/ InP (100) quantum dot laser emitting around 1.55 µm," *Electronics Letters,* vol. 44, pp. 522-523, 2008.

[13] B. W. Tilma, M. S. Tahvili, J. Kotani, R. Nötzel, M. K. Smit, and E. A. J. M. Bente, "Measurement and analysis of optical gain spectra in 1.6 to 1.8 µm InAs/InP (100) quantum-dot amplifiers," *Optical and Quantum Electronics,* vol. 41, pp. 735-749, Aug 2009.

[14] G. T. Liu, A. Stintz, H. Li, T. C. Newell, A. L. Gray, P. M. Varangis, K. J. Malloy, and L. F. Lester, "The influence of quantum-well composition on the performance of quantum dot lasers using InAs-InGaAs dots-in-a-well (DWELL) structures," *Quantum Electronics, IEEE Journal of,* vol. 36, pp. 1272-1279, 2000.

[15] J. Kotani, P. J. van Veldhoven, T. de Vries, B. Smalbrugge, E. A. J. M. Bente, M. K. Smit, and R. Nötzel, "First demonstration of single-layer InAs/InP (100) quantum-dot laser: continuous wave, room temperature, ground state," *Electronics Letters,* vol. 45, pp. 1317-1318, Dec 3 2009.

[16] O. B. Shchekin and D. G. Deppe, "Low-threshold high-T/sub 0/ 1.3-/spl mu/m InAs quantum-dot lasers due to p-type modulation doping of the active region," *Photonics Technology Letters, IEEE,* vol. 14, pp. 1231-1233, 2002.

[17] G. Ozgur, A. Demir, and D. G. Deppe, "Threshold Temperature Dependence of a Quantum-Dot Laser Diode With and Without p-Doping," *Quantum Electronics, IEEE Journal of,* vol. 45, pp. 1265-1272, 2009.

[18] M. Mitsuhara, M. Ogasawara, M. Oishi, H. Sugiura, and K. Kasaya, "2.05-µm wavelength InGaAs-InGaAs distributed-feedback multiquantum-well lasers with 10-mW output power," *Photonics Technology Letters, IEEE,* vol. 11, pp. 33-35, 1999.

[19] T. Sato, M. Mitsuhara, and Y. Kondo, "InAs Quantum-well Distributed Feedback Lasers Emitting at 2.3 µm for Gas Sensing Applications," *NTT Technical Review,* vol. 7, 2009.

[20] T. Sato, K. Mitsuhara, T. Watanabe, K. Kasaya, T. Takeshita, and Y. Kondo, "2.1-µm-Wavelength InGaAs Multiple-Quantum-Well Distributed Feedback Lasers Grown by MOVPE Using Sb Surfactant," *Selected Topics in Quantum Electronics, IEEE Journal of,* vol. 13, pp. 1079-1083, 2007.

[21] B. W. Hakki and T. L. Paoli, "Gain spectra in GaAs double - heterostructure injection lasers," *Journal of Applied Physics,* vol. 46, pp. 1299-1306, 1975.

[22] A. Oster, G. Erbert, and H. Wenzel, "Gain spectra measurements by a variable stripe length method with current injection," *Electronics Letters,* vol. 33, pp. 864-866, 1997.

[23] J. D. Thomson, H. D. Summers, P. J. Hulyer, P. M. Smowton, and P. Blood, "Determination of single-pass optical gain and internal loss using a multisection device," *Applied Physics Letters,* vol. 75, pp. 2527-2529, 1999.

[24] M. Sugawara, N. Hatori, H. Ebe, M. Ishida, Y. Arakawa, T. Akiyama, K. Otsubo, and Y. Nakata, "Modeling room-temperature lasing spectra of 1.3-mu m self-assembled InAs/GaAs quantum-dot lasers: Homogeneous broadening of optical gain under current injection," *Journal of Applied Physics,* vol. 97, pp. 043523-8, 2005.

[25] M. Gioannini, A. Sevega, and I. Montrosset, "Simulations of differential gain and linewidth enhancement factor of quantum dot semiconductor lasers," *Optical and Quantum Electronics,* vol. 38, pp. 381-394, 2006.

[26] M. Gioannini and I. Montrosset, "Numerical analysis of the frequency chirp in quantum-dot semiconductor lasers," *Quantum Electronics, IEEE Journal of,* vol. 43, pp. 941-949, 2007.

[27] N. Tansu and L. J. Mawst, "Current injection efficiency of InGaAsN quantum-well lasers," *Journal of Applied Physics,* vol. 97, pp. 054502-18, 2005.

[28] H. Zhao, G. Liu, R. A. Arif, and N. Tansu, "Current injection efficiency induced efficiency-droop in InGaN quantum well light-emitting diodes," *Solid-State Electronics,* vol. 54, pp. 1119-1124, 10// 2010.

[29] M. Rossetti, P. Bardella, M. Gioannini, and I. Montrosset, "Carrier Transport Effects in Multi Layer Quantum Dot Lasers and SLDs," in *Proceedings of the 14th European Conference on Integrated Optics and Technical Exhibition (ECIO 2008)*, Eindhoven, the Netherlands, 2008.

[30] M. Rossetti, P. Bardella, and I. Montrosset, "Time-Domain Travelling-Wave Model for Quantum Dot Passively Mode-Locked Lasers," *Quantum Electronics, IEEE Journal of,* vol. 47, pp. 139-150, 2011.

[31] F. Grillot, K. Veselinov, M. Gioannini, I. Montrosset, J. Even, R. Piron, E. Homeyer, and S. Loualiche, "Spectral Analysis of 1.55-µm InAs-InP(113)B Quantum-Dot Lasers Based on a Multipopulation Rate Equations Model," *Quantum Electronics, IEEE Journal of,* vol. 45, pp. 872-878, 2009.

[32] Z. Y. Xu, Z. D. Lu, X. P. Yang, Z. L. Yuan, B. Z. Zheng, J. Z. Xu, W. K. Ge, Y. Wang, J. Wang, and L. L. Chang, "Carrier relaxation and thermal activation of localized excitons in self-organized InAs multilayers grown on GaAs substrates," *Physical Review B,* vol. 54, p. 11528, 1996.

[33] H. Lee, W. Yang, and P. C. Sercel, "Temperature and excitation dependence of photoluminescence line shape in InAs/GaAs quantum-dot structures," *Physical Review B,* vol. 55, p. 9757, 1997.

[34] W. Ouerghui, A. Melliti, M. A. Maaref, and J. Bloch, "Dependence on temperature of homogeneous broadening of InGaAs/InAs/GaAs quantum dot fundamental transitions," *Physica E: Low-dimensional Systems and Nanostructures,* vol. 28, pp. 519-524, 2005.
[35] J. P. Weber, "Optimization of the carrier-induced effective index change in InGaAsP waveguides-application to tunable Bragg filters," *Quantum Electronics, IEEE Journal of,* vol. 30, pp. 1801-1816, 1994.